Tropical Clouds and Circulation Changes During the 2006-07 and 2009-10 El Niños

Hui Su and Jonathan H. Jiang

Jet Propulsion Laboratory, California Institute of Technology, Pasadena, California 91109, USA

Corresponding Email: Hui.Su@jpl.nasa.gov

Abstract: Changes in tropical cloud vertical structure, cloud radiative forcing (CRF) and circulation exhibit distinctly different characteristics during the 2006-07 and 2009-10 El Niños, revealed by CloudSat/CALIPSO observations and reanalysis data. The 2009-10 El Niño produces a strong increase of deep convection over the equatorial central Pacific but wide-spread decreases of convection in other ocean basins. The 2006-07 El Niño produces moderate enhancement of convection in central and eastern Pacific but relatively confined reduction of convection. In the tropical average, the 2009-10 has a decrease of mid-to-high clouds and an increase of low clouds. The 2006-07 experiences nearly the opposite. The tropical averaged net CRF anomaly at the top-of-the-atmosphere (TOA) is 0.6-0.7 W/m^2 *cooling* (0.2-0.5 W/m^2 *warming*) for the 2009-10 (2006-07) El Niño. The 2009-10 El Niño is associated with a strengthening of tropical circulation, increased high (low) clouds in extremely strong ascending (descending) regimes and decreased mid-to-high clouds in a broad range of moderate circulation regimes. The strengthening of tropical circulation is primarily contributed by the enhancement of the Hadley circulation. The 2006-07 El Niño is associated with a weakening of tropical circulation, primarily contributed by the reduction of the Walker circulation. The cloud anomalies in each circulation regime are approximately opposite to those in 2009-10. Our analysis suggests that both magnitude and pattern of sea surface temperature anomalies in the two events contribute to the differences in clouds and circulation anomalies, with magnitude playing a dominant role. The contrasting behaviors of the two El Niños highlight the nonlinear response of tropical clouds and circulation to El Niño SST forcing.

1. Introduction

On interannual time scale, El Niño–Southern Oscillation (ENSO) is the most dominant natural variability. ENSO is characterized by anomalous sea surface temperature (SST) in the equatorial Pacific and has far-reaching impacts on global and regional temperature, precipitation and circulation. Changes in tropical clouds during ENSO have been studied extensively (e.g. Ramanathan and Collins 1991; Zhang et al; 1996; Cess et al., 2001; Allan et al., 2002) owing to the profound importance of clouds on the Earth's radiative energy balance. At the time when no direct observation of cloud vertical profiles on the tropical/global scale was available, a few studies used the ratio of shortwave and longwave cloud forcing (SWCF and LWCF) at the top-of-atmosphere (TOA), N = –SWCF/LWCF, to infer cloud height for the understanding of TOA cloud radiative forcing (CRF) changes. There has been a controversy whether the abnormally large N value over the western Pacific warm pool during the 1998 El Niño was dominated by lowering of deep convective cloud heights (Cess et al., 2001) or increasing low-level clouds associated with anomalous subsidence (Allan et al, 2002). Yuan et al. (2008) revisited the issue by analyzing the International Satellite Cloud Climatology Project (ISCCP) cloud fraction data along with the CRF estimates from the Earth Radiation Budget Experiment (ERBE) and the Clouds and the Earth's Radiant Energy System (CERES) as a function of large-scale vertical motion, following the methodology put forward by Bony et al. (2004). Their results showed that both high and low clouds underwent significant changes during the 1998 El Niño and the shift from "top-heavy" to "bottom-heavy" upward motion in the western Pacific appeared to be responsible for the cloud vertical structure change, rather than the mean vertical motion.

CloudSat and Cloud-Aerosol Lidar and Infrared Pathfinder Satellite (CALIPSO) experiments have conducted global survey of cloud vertical profiles since 2006. These measurements enable us to unambiguously identify changes of cloud vertical structure in response to El Niño. During

CloudSat/CALIPSO observational period, two El Niños occurred. Based on the difference in SST anomalies averaged over the Niño4 (160°E–150°W, 5°S–5°N) and Niño3 (150°–90°W, 5°S–5°N) regions, the two EL Niños were classified as two types of El Niño (Yeh et al. 2009; Lee and McPhaden 2010). The 2006-07 El Niño was a moderate Eastern Pacific (EP)-El Niño, characterized by warm SST anomalies across the eastern and central Pacific with Niño3 SST anomaly greater than that over Niño4. In contrary, the winter of 2009-10 experienced large positive SST anomalies over the central Pacific with Niño4 SST anomaly significantly higher than Niño3, making it the strongest Central Pacific (CP)-El Niño since 1980s (Lee and McPhaden 2010). The CP-El Niño is also called El Niño Modoki and is associated with different even opposite teleconnection patterns from the canonical EP-El Niño (Latif et al. 1997; Ashok et al. 2007; Kao and Yu 2009; Kug et al. 2009; Weng et al. 2007; Weng et al. 2009; Kim et al. 2009). With CloudSat/CALIPSO cloud profile observations, we now have a clear view of 3-dimensional cloud structure during the two types of El Niño. The purpose of this paper is to document and understand cloud vertical structure changes during the two El Niños. As tropical clouds are intimately coupled with large-scale circulation, we also analyze tropical circulation changes. Since these two events differ both in SST anomaly pattern and magnitude, we diagnose the relative roles of SST anomaly pattern and magnitude in determining the clouds and circulation responses in the tropics. Our analysis results encompass cloud and circulation changes in conventional geographical space and in large-scale dynamic regimes, indicated by mid-tropospheric vertical pressure velocity at 500 hPa (ω_{500}).

A major limitation of using CloudSat/CALIPSO data to examine interannual cloud changes is the short time span of the data record. We construct monthly anomalies relative to the mean seasonal cycle based on the four year data from August 2006 to July 2010. This period includes two warm and two cold episodes of ENSO, making a nearly neutral climatology. To test the

robustness of the anomalies, we compare our CloudSat/CALIPSO cloud fraction (CFr) anomalies with satellite record of longer temporal coverage, such as the CFr data from ISCCP, recognizing the coarse vertical stratification of the latter. We also compare the short-term (August 2006 - July 2010) and long-term mean atmospheric circulation (1981-2010) from the European Centre for Medium-Range Weather Forecasts (ECMWF) interim reanalysis. Given the similarity between such short-term and long-term means, we are assured that the relatively short record of CloudSat/CALIPSO observation is useful in studying interannual variabilities.

The structure of the paper is organized as follows. Section 2 describes the data used in the analysis. Section 3 presents the clouds and circulation anomalies during the two El Niños in geographical space, while Section 4 presents cloud changes in the functional space of large-scale circulation and diagnosis of whether the pattern or magnitude of SST anomaly determines the different responses. The TOA cloud forcings for the two events are discussed in Section 5. Concluding remarks are given in Section 6.

2. Data

The cloud profile data we use include cloud water content (CWC) from CloudSat Level 2B-CWC-RO and CloudSat radar and CALIPSO lidar combined cloud fraction retrieval from 2B-GEOPROF-LIDAR. The vertical resolution of these data is about 500 m, oversampled onto 250 m intervals from surface to 20 km. The horizontal resolution is 1.7 km along track and 1.3 km cross track. The uncertainty of CWC is about a factor of 2 (Jiang et al. 2012). CWC retrievals within 0.5 km above the surface are not used because of the large uncertainties due to surface clutter. To validate the spatial patterns of CloudSat/CALIPSO cloud data, we employ the ISCCP cloud fraction from July 1983 to December 2009. This version of ISCCP data is the latest release of ISCCP D2 global monthly dataset. The horizontal resolution of the original data is 280 km × 280 km.

To derive TOA CRF, we use monthly 1ºx1º gridded all-sky and clear-sky radiative flux measurements from CERES on Terra and Aqua (the SYN1deg-Month-lite Edition 2.5-Subset Data). The uncertainties for monthly and regional mean CERES TOA longwave and shortwave fluxes are about 0.2-0.4 W/m^2 [*Loeb et al*., 2007].

SST data are from the NOAA Optimum Interpolation SST, and atmospheric winds are from the ECMWF interim reanalysis with a horizontal resolution of 1.5º×1.5º.

3. Cloud and Circulation Changes

As maximum El Niño warming usually occurs in boreal winter, we focus on the cloud and circulation anomalies averaged for December, January and February (DJF). Figure 1 shows the spatial distributions of SST anomalies relative to the four DJF means from 2006 to 2010 for the two El Niño winters. The SST anomalies relative to 30-year mean (1981-2010) are very similar (figure not shown). In 2009-10 DJF, the positive SST anomalies are concentrated between the dateline and 120ºW, while the warm anomalies during 2006-07 DJF are wide-spread across the eastern-central Pacific despite of the maximum around 180º. The tropical (30°S-30°N) averaged SST anomalies are 0.3°C for 2009-10 DJF and 0.1°C for 2006-07 DJF.

Figure 2 shows the anomalies of tropical (30°S-30°N) averaged cloud water content (CWC) and CFr profiles over the tropical oceans for the four winters, with the tropical mean SST anomalies in each winter displayed in the inset. The tropical averaged cloud anomalies for the two El Niños are almost opposite to each other over most of the troposphere, with an overall reduction of cloudiness in 2009-10 and an increase in 2006-07. At the altitudes above 14 km (below 1.5 km), both 2009-10 and 2006-07 experience an increase of cirrus (low clouds) in CWC. The changes in CFr are consistent with those in CWC, but extend higher in altitude than in CWC, because of the higher sensitivity of the lidar to thinner clouds than the radar. The amplitude of the CWC (CFr) anomaly in the tropical average is about 1 mg/m^3 (0.5%).

Compared to the four-year mean, the fractional difference is up to 5-10% for CWC and 15-30% for CFr in the free troposphere (2-14 km). For the two La Niñas (note that the 2008-09 winter was not regarded as a persistent cold episode because the SST anomalies were not over the threshold of –0.5ºC for a minimum of five consecutive over-lapping seasons (http://www.cpc.ncep.noaa.gov/products/analysis_monitoring/ensostuff/ensoyears.shtml), reduced high clouds (above 10-12 km) and increased middle clouds (2-10 km) are observed, while low clouds (below 2 km) are reduced during 2007-08 but increased slightly during 2008-09 (with reduced CFr). If we restrict the spatial averages to the Pacific Ocean only (120ºE-90ºW) (figure not shown), the cloudiness anomalies are of the same sign, but with smaller amplitude, indicating that the cloud anomalies over the Pacific Ocean are dominant in the tropical average but contributions from other ocean basins are important (Zhang et al., 1996).

The horizontal distributions of CWC and CFr anomalies at four pressure levels are shown in Figure 3. The four levels represent the planetary boundary layer, middle and upper troposphere, and the tropopause region. At 900 hPa, the two El Niños exhibit a striking contrast with the cloud anomalies of opposite sign over most of the tropics. In the equatorial southeast Pacific, the 2006-07 El Niño produces a decrease of low clouds, with only a small area of increased low clouds adjacent to the west coast of Peru and Chili. The 2009-10 El Niño, on the contrary, has a strong positive anomaly of low clouds. The magnitude of increased low clouds is about 15% in cloud fraction and 20 mg/m^3 (more than double the 4-year mean). This increase of low cloud amount has a substantial contribution to the net cloud forcing in the tropics. It may be related to the local negative SST anomalies observed during DJF 2009-10 (see Figure 1), although it is not clear whether the cold SST anomalies are the consequence of reduced downward solar radiation at the surface associated with the increased low clouds. In the equatorial northeast Pacific, the low cloud anomalies are positive in DJF 2006-07 but negative in DJF 2009-10. This short-term

157 variability seems to be at odds with long-term trends of low cloud variations over this area as
158 documented in Clement et al. (2009). Detailed analysis is needed to understand the mechanisms
159 that drive the low cloud changes.

160 From 600 hPa to 100 hPa, cloud anomalies are approximately barotropic, because the
161 changes of deep convective strength dominate the cloud response. The cloud anomalies are
162 substantial at 200 hPa (~10km). Interestingly, both El Niños have maximum positive cloud
163 anomalies near the dateline, with the 2009-10 maximum located more towards the south of the
164 equator than the 2006-07 maximum. To the east of the maximum positive cloud anomaly in the
165 Pacific, the two El Niños are more or less similar; however, to the west of the maximum, the two
166 El Niños are drastically different. Over the western Pacific and maritime continent, strong
167 negative high cloud anomalies occur in the winter of 2009-10, comparing to the positive high
168 cloud anomalies in DJF 2006-07. Over most of the Indian Ocean, 2006-07 winter experiences
169 enhanced convection, while 2009-10 winter shows reduced convection. Opposite cloud
170 anomalies also appear in the equatorial Atlantic Ocean for the two events. At 600 hPa and 100
171 hPa, cloud anomalies outside the Pacific Ocean are much smaller than those inside the Pacific.
172 During DJF 2009-10, the 100 hPa cloud fraction and CWC anomalies over the Indian and
173 Atlantic Oceans are positive while their counterparts at 200 hPa are negative, suggesting that
174 cirrus variations are not fully determined by changes in deep convection.

175 The robustness of the CloudSat/CALIPSO anomaly pattern is tested in Figure 4 using the
176 cloud fraction data from ISCCP. We display the ISCCP cloud fraction anomalies for December
177 2006 and 2009 relative to the December mean based on long-term (1983-2009) and short-term
178 (2006-2009) averages. Similar to Clement et al. (2009), we add ISCCP low and middle cloud
179 fraction together because of the uncertainty in the retrieval of low-level cloud top height. It is
180 clear that the cloud fraction anomalies using different means are very similar. The spatial

distributions of cloud fraction anomalies generally agree with those of CloudSat/CALIPSO, although it is not meaningful to quantify the differences due to the broad classification of vertical layers in the ISCCP data.

As the changes of tropical cloud anomalies are strongly correlated with changes in tropical circulation, we plot the tropical 3-d wind anomalies using ECMWF interim reanalysis together with cloud anomalies from CloudSat/CALIPSO. Figure 5 is the longitude-height section for anomalies averaged over 10ºS-10ºN. Figure 6 is a latitude-height section for zonally averaged anomalies. Only oceanic regions are included in the averages. In both figures, the vertical wind (in hPa/day) is enlarged 5000 times to stress the overturning circulation.

On the zonal plane (Figure 5), the 2006-07 El Niño has a widespread increase of mid-to-high clouds across the central and eastern Pacific, while the 2009-10 El Niño has a much stronger positive deep convective cloud anomaly near the dateline. The increase of deep convection is associated with enhanced ascending motions. The high vertical resolution of CloudSat/CALIPSO data reveals the fine structure of anomalous cloud profiles that are not available from previous datasets such as the ISCCP. For example, the positive high cloud fraction anomalies above 200 hPa in the central Pacific during DJF 2009-10 exhibit an eastward tilting with height, indicating the role of horizontal winds in advecting detrained ice clouds. During both El Niños, some negative cloud anomalies are underneath or in-between moderately strong positive anomalies, creating a rather inhomogeneous response in the vertical. During DJF 2006-07, the compensating subsidence in response to the enhanced ascent is confined within the western Pacific around 90ºE-135ºE, while the 2009-10 has a far-reaching forced descent over the Indian (45º-90ºE) and Atlantic (300º-360º) Oceans beyond the western Pacific. Over the Indian Ocean, the two El Niño winters have opposite cloud anomalies although the local SST anomalies are both positive. This

is a clear manifestation of the "atmospheric bridge", i.e, the remote impact of ENSO SST through atmospheric circulation (Alexander et al. 2002; Su et al. 2001).

On the meridional plane (Figure 6), the differences between the two El Niños are evident. The 2006-07 has the maximum anomalous upward motion located to the north of the equator. The compensating subsidence is restricted within 15 degrees of the maximum ascending anomaly. Poleward of 15ºS and 20ºN, circulation anomalies are relatively weak, accompanied by increased middle and high clouds. On the other hand, the 2009-10 El Niño has a maximum of enhanced ascent to the south of the equator. It induces strong descent anomalies poleward of 10ºS and 5ºN, generating strong negative cloud anomalies. In the boundary layer, low clouds anomalies are opposite for the two events, consistent with the large-scale circulation change and probably correlated with the variations of lower tropospheric stability.

4. Cloud changes in the large-scale circulation regimes

Following *Bony et al.* (2004), we treat tropical cloudiness as a function of ω_{500}. In this framework, the tropical mean cloudiness (<*C*>) is expressed as an integral of cloudiness in each circulation regime (C_ω), weighted by the probability density function (pdf) of each regime (P_ω), i.e., $< C >= \int_{-\infty}^{+\infty} P_\omega C_\omega d\omega$. Thus, the change of tropical mean cloudiness from climatology can be decomposed into a term associated with the change of large-scale circulation (termed dynamic component), $C_1 = \int_{-\infty}^{+\infty} \delta P_\omega \cdot C_\omega d\omega$; a term associated with the change of cloudiness in each regime (termed thermodynamic component), $C_2 = \int_{-\infty}^{+\infty} P_\omega \cdot \delta C_\omega d\omega$; and the co-variation between the two, $C_3 = \int_{-\infty}^{+\infty} \delta P_\omega \cdot \delta C_\omega d\omega$, where δP_ω and δC_ω are anomalies from their climatological means. Hence,

the tropical mean cloud change $<\delta C>=\int_{-\infty}^{+\infty}\delta P_\omega \cdot C_\omega d\omega+\int_{-\infty}^{+\infty}P_\omega \cdot \delta C_\omega d\omega+\int_{-\infty}^{+\infty}\delta P_\omega \cdot \delta C_\omega d\omega$. We note that the terminologies (dynamic and thermodynamic components) should not be interpreted literally, as the C_1 and C_2 terms are strongly correlated, both being driven by SST anomalies.

Figure 7 shows tropical cloudiness (CWC in color shadings and CFr in line contours) sorted in 20 bins of ω_{500} with a bin interval of 10 hPa/day for the two El Niños. Figure 7a,b are total cloud amount and 7c,d are cloud anomalies relative to the 4 DJF means. The three components of cloud anomalies are shown in Figure 8.

As the SST anomalies are stronger in 2009-10 than in 2006-07, high clouds in the strongly ascending regimes appear higher in altitude and greater in magnitude in both CWC and CFr. The intense high clouds are more concentrated over strongly ascending regimes ($\omega_{500} < -75$ hPa/day) in 2009-10, whereas they span a broader range of ascending regimes in 2006-07 (Figure 7a-b). The shift to stronger ascending regimes and to higher altitudes in 2009-10 is clearly manifested in the anomalous cloudiness distributions (Figure 7c-d). The 2009-10 El Niño shows an increase of high clouds in the strongly ascending regime where ω_{500} is less than −75 hPa/day, and a substantial decrease of mid-to-high cloudiness in the moderate circulation regimes, spanning ω_{500} between −75 and 20 hPa/day (Figure 7d). Such a decrease in high- and mid-level clouds in the intermediate circulation regimes is a result from the shift of high cloudiness to stronger ascending regime. There is also a decrease in boundary layer clouds in the moderate subsidence regimes with ω_{500} less than 20 hPa/day. In the strongly descending regimes with ω_{500} between 20 and 60 hPa/day, low clouds and middle clouds are increased. Changes of clouds in the regimes of $\omega_{500} > 60$ hPa/day are quite small. These cloud anomalies are associated with the changes in the pdf of ω_{500} (δP_ω) which exhibit a polarizing feature: an increase at two extremes and a decrease

246 over the broad range of intermediate ω_{500}, corresponding to a strengthened tropical circulation
247 (Figure 9a). As the moderate ω_{500} values ($-75 < \omega_{500} < 20$ hPa/day) account for about 60% of
248 tropical circulation regimes and the relatively large magnitude of cloud anomalies there, the
249 tropical-mean CWC and CFr show a reduction of clouds throughout the troposphere, except
250 below 1 km and above 14 km. The three components (C_1, C_2 and C_3) of cloud changes (Figure
251 8d-f) indicate that the both dynamic (C_1) and thermodynamic (C_2) components contribute to the
252 sandwich-like structure in Figure 7d and that thermodynamic component (C_2) dominates the sum
253 of the three terms.

254 On the contrary, during the 2006-07 El Niño, high and middle clouds are reduced over the
255 strongly ascending regimes but increased in the moderate circulation regimes (Figure 7c),
256 associated with an increase in the pdf of intermediate ω_{500} values and an decrease at both
257 extreme ranges, opposite to the 2009-10 El Niño. Hence, the tropical-mean high and middle
258 clouds are increased relative to the 4-year mean. The changes in the ω_{500} pdf indicate a
259 weakening of tropical circulation (Figure 9a), which resembles climate model simulated
260 circulation changes in response to uniform SST warming [*Bony et al*., 2004]. The individual
261 components (C1 and C2) are largely mirror images of those in 2009-10 but of opposite signs
262 (Figure 8a-c).

263 Following *Held and Soden* (2006), we compute the spatial variance of ω_{500} ($<\omega_{500}^{*\,2}>$) over
264 the entire tropics (30ºS-30ºN) and divide it into the zonally symmetric component ($<\overline{\omega_{500}^{*}}^{2}>$) and
265 asymmetric component ($<\omega_{500}'^{\,2}>$), to represent the strength of Hadley and Walker circulations,
266 respectively (Figure 9b), i.e., $<\omega_{500}^{*\,2}> = <\overline{\omega_{500}^{*}}^{2}> + <\omega_{500}'^{\,2}>$. The asterisk, over-bar and prime
267 denote the departure from the tropical mean, the zonal-mean and the departure from the zonal-
268 mean, respectively. Note that such definitions of the Hadley and Walker circulation indices are

different from other commonly used indices [e.g., *Oort and Yienger*, 1996; *Tanaka et al*., 2004; *Quan et al*., 2004; *Mitas et al*., 2005] but they form a closed budget for the total spatial variance of ω_{500} in the tropics. Thus, the "Hadley Circulation" and "Walker Circulation" defined here loosely correspond to the mean tropical circulation on the meridional plane and zonal plane, respectively. We find that during 2009-10 DJF the strengthening of the Hadley circulation explains 90% of the increased spatial variance of ω_{500}, while the rest is contributed by the strengthening of the Walker circulation. During 2006-07 DJF, the weakening of circulation is primarily due to the weakening of the Walker circulation, while the weakening of the Hadley circulation accounts for 10% of the decreased spatial variance of ω_{500}. For the 2007-08 and 2008-09 La Niñas, the Walker circulation is strengthened but the Hadley Circulation is weakened. The changes in the strength of the Hadley and Walker circulations during ENSO have been documented before [*Oort and Yienger*, 1996; *Tanaka et al*., 2004]; however, the changes in the strength of the Hadley and Walker circulations for the two El Niños analyzed here are not inversely correlated as for most historical El Niños, indicating the varying nature of El Niños.

What causes the distinctly different responses in clouds and large-scale circulation during 2009-10 and 2006-07 El Niños? We perform a diagnosis to illustrate the differences in SST anomalies between the two events. Considering the SST gradient is crucial to determine the tropical circulation and deep convection (*Lindzen and Nigam* 1987), previous studies (*Bony et al.* 2004, *William et al*. 2003) suggested that the relative warmth of local SST, i.e., the departure of local SST from the tropical-mean SST ($\delta SST_i = SST_i - < SST >$ for the ^{i}th grid-box), correlates better with the local cloud change. We analyze the distributions of δSST and find that the changes in the occurrence frequency of δSST in three broadly defined regimes bear approximate similarity to the changes in the pdf of ω_{500} (Figure 10a). During 2009-10, there is an increase in

292 the occurrence of strongly relatively warm SSTs with δSST > 2.4ºC, approximately the upper
293 ~20% of the δSST distribution, accompanied by a decrease in the occurrence of intermediate
294 δSST values (between -2.2 and 2.4ºC) and an increase in the occurrence of strongly relatively
295 cold SSTs. The positive SST anomalies during DJF 2006-07 are wide-spread over the central and
296 eastern Pacific, leading to a reduced SST gradient: the pdf of the extremely relatively warm
297 δSST decreases and the pdf of the intermediate δSST increases.

298 However, the two El Niños also differ in the magnitude of positive SST anomalies. To
299 distinguish the role of SST anomaly magnitude and pattern in determining the δSST distribution,
300 we keep the spatial distributions of SST anomalies during DJF 2006-07 but enlarge their
301 magnitudes so that the tropical-mean SST anomalies are of the same magnitude for DJF 2006-07
302 and 2009-10. After this manipulation, the anomaly of δSST occurrence frequency for 2006-07
303 changes to a polarized structure, qualitatively similar to that in 2009-10 (Figure 10b). This
304 exercise suggests that the larger magnitude of SST anomalies during DJF 2009-10 is the key to
305 the strengthened circulation and associated cloud anomalies, although the pattern of SST may
306 also play a role.

307 **5. TOA cloud forcings**

308 Given the drastically different cloud anomalies during the two El Niños, it is expected large
309 differences would incur in their TOA cloud forcings. We analyze TOA CRFs from CERES on
310 Terra and Aqua both in the geographical space and in the large-scale circulation regimes. We
311 define CRF as the difference between the all-sky and clear-sky TOA radiative fluxes, with the
312 positive sign indicating warming to the Earth-atmosphere system. The spatial maps of longwave,
313 shortwave and net cloud forcing anomalies as well as the anomalies of ratio N are shown in
314 Figure 11 and the regime-sorted CRF for both El Niños are shown in Figure 12. Table 1

315 summarizes cloud forcing anomalies in different circulation regimes. The anomalies are relative
316 to the four winters from 2006-2010. They are similar to the anomalies relative to 10 (8) years
317 mean for Terra (Aqua) CERES data.

318 The pattern of LWCF anomalies resembles that of cloud anomalies at 200 hPa (Figure 3),
319 while the shortwave cloud forcing shows combined effects of high, middle and low cloud
320 anomalies. Interestingly, the net cloud forcing has a similar spatial distribution to the cloud
321 anomalies at 600 hPa, except over the substantial low cloud anomaly regions (i.e., the west coast
322 of South America and Australia). This suggests that middle clouds have an important
323 contribution to the net cloud forcing as the LWCF and SWCF from high clouds nearly cancel
324 each other. The ratio N exhibits appreciable anomalies over regions of relatively large low cloud
325 anomalies, but it has small changes over regions of deep convection such as the western Pacific
326 and the Indian Ocean, indicating the limitation of using this ratio to infer cloud structure
327 changes.

328 Sorting CRF in the large-scale circulation regimes discloses, to some degree, the
329 contributions of each type of clouds to the total cloud forcing. During 2009-10 DJF, the
330 increased deep clouds in the strongest ascending regimes ($\omega_{500} < -75$ hPa/day) produce enhanced
331 shortwave cooling and longwave warming at the TOA, with the shortwave cooling dominating.
332 In the intermediate circulation regimes, the reduction of mid-to-high clouds leads to decreased
333 shortwave cooling (positive anomaly) and decreased longwave warming (negative anomaly), i.e.,
334 resulting in an anomalous cooling effect. In the strongest descending regimes ($\omega_{500} > 20$
335 hPa/day), the increased low cloudiness causes an increased shortwave cooling. On the tropical
336 average, the net CRF is a cooling of 0.6-0.7 W/m^2, to which the low clouds over the subsidence
337 regimes contribute about 70-80% (Table 1). Compared to 2009-10, the 2006-07 DJF shows
338 nearly opposite longwave and shortwave CRF changes in the intermediate circulation regimes (–

339 $75 < \omega_{500} < 0$ hPa/day), consistent with the observed cloud changes. The tropical-mean net CRF
340 anomaly during 2006-07 is 0.2-0.5 W/m^2 warming based on the two CERES datasets, with the
341 averages for the large-scale ascending and descending regimes counteracting each other (0.3-0.4
342 W/m^2 cooling versus 0.5-0.9 W/m^2 warming). The differences in CRF between the Terra and
343 Aqua CERES data are within the uncertain range of 0.2-0.4 W m^{-2}.

344 During both El Niños, low clouds in the subsidence regimes are the primary contributor to
345 the tropical-mean cloud forcing, consistent with previous studies [e.g., *Bony and Dufrescne*,
346 2005]. However, the contribution of mid-to-high clouds in the ascending regimes to the tropical-
347 mean CRF is non-negligible. In both ascending and descending regimes, the SWCF outweighs
348 the LWCF, except during 2009-10 in the ascending regime. Our estimates of cloud sensitivity to
349 ENSO SST warming are of approximately similar magnitude to the previous estimates of 1-2
350 Wm^{-2}K^{-1} [e.g. *Zhang et al*., 1996], although the sign may vary from case to case.

351 **6. Concluding remarks**

352 With vertically resolved cloud water content and cloud forcing profiles observed by
353 CloudSat/CALIPSO, we are able to, for the first time, quantify the vertical variations of clouds in
354 response to El Niño SST warming. Two El Niños are examined and compared. We conclude that
355 the magnitude and pattern of SST anomalies are both important to the tropical-mean cloud
356 amount change. In the winter of 2009-10, the tropical-mean SST anomaly is about 3 times of that
357 in the winter of 2006-07 and the warmest anomalies are concentrated over the central Pacific,
358 where climatological SST is warm. Consequently, the strong anomalous ascent over the central
359 Pacific moves deep convective clouds higher in altitude and induce strong descent anomaly
360 remotely, causing wide-spread decrease of deep convective clouds in tropical oceans. The
361 zonally overturning circulation (i.e., the Walker Circulation) shifts the ascending branch from
362 western Pacific to the central Pacific and greatly enhances the descending branch to the west

(into the Indian Ocean), resulting in little reduction in overall zonal circulation strength as indicated by the zonally asymmetric component of the spatial variance of ω_{500}, while the meridionally overturning circulation (i.e. the Hadley Circulation) strengthens due to the increased meridional SST gradient. On the other hand, the 2006-07 represents more of canonical El Niño, during which the Walker circulation weakens and the Hadley circulation is less affected. The differences between the two El Niños highlight the nonlinearity in the ENSO response (Hoerling et al., 1997). Hence, it is probably not surprising that global or tropical mean cloud forcing shows a large scatter with respect to the mean surface temperature anomalies (Dessler 2010) on the interannual time scale, a characteristic manifested in tropical-mean precipitation (e.g., Su and Neelin 2003, Gu et al. 2007).

Besides large differences in high and middle cloud anomalies, low clouds over the west coast of South America and Australia and subtropical Pacific also exhibit nearly opposite responses to the two El Niños. Although low cloud observations are more difficult to confirm using longer historical data, the consistency in spatial patterns of TOA cloud forcing anomalies validates the CloudSat/CALIPSO low cloud retrievals. As these low cloud anomalies make a dominant contribution to the net cloud forcing at the TOA, an in-depth analysis of the physical processes responsible for the low cloud change is warranted.

Although a single El Niño event does not bear any indication of future climate change, it is interesting to point out that this new type of El Niño Modoki, or the CP El Niño, may have increasing importance in future climate variabilities. It has been suggested that the occurrence of EP-El Niño has become less frequent and the CP-El Niño has become more common during the late twentieth century (*Latif et al*. 1997; *Ashok et al*. 2007). The intensity of CP-El Niño has also increased since the 1990s (*Lee and McPhaden* 2010). Coupled climate model simulations projected that the occurrence ratio of CP-El Niño to EP-El Niño would increase as much as five

387 times under global warming (*Yeh et al*. 2009). Hence, investigations of the CP-El Niño and its
388 global impacts, in contrast to EP-El Niño, are important to understanding interannual and longer-
389 term climate variabilities. A recent study by Zelinka and Hartmann (2011) regressed 8 years A-
390 Train cloud observations since 2002 against tropical-mean SST and found a decrease of high
391 clouds in response to SST warming, qualitatively similar to the cloud response during the 2009-
392 10 El Niño shown in this study. This might suggest that the CP-El Niño occurred more
393 frequently than the EP-El Niño in the past decade.

394 The magnitude and pattern dependency of the tropical or global mean cloud forcing presents
395 a great challenge to the determination of cloud feedback as climate models have yet agreed on
396 the regional-scale (a few thousand kilometers, for example, Central Pacific versus Eastern
397 Pacific) surface temperature changes [*Merryfield*, 2006], let alone on the local scale (a few
398 hundred kilometers). Moreover, the height dependency of cloud response to surface warming
399 also makes the accurate quantification of cloud feedback very difficult. Measurements of TOA
400 radiative fluxes only provide the 2-dimensional constraint on cloud forcing. To fully understand
401 and determine cloud feedback, accurate global measurement of 3-dimensional cloud structure is
402 needed.

403 **Acknowledgment**. We thank T. J. Shen for help with data analysis and thank G. Stephens, J. D.
404 Neelin and K. Minschwaner for helpful discussions. We are especially grateful to D. Vane for
405 funding support. This work was performed at Jet Propulsion Laboratory, California Institute of
406 Technology, under contract with NASA.

407

References

Alexander, Michael A., Ileana Bladé, Matthew Newman, John R. Lanzante, Ngar-Cheung Lau, James D. Scott, 2002: The Atmospheric Bridge: The Influence of ENSO Teleconnections on Air–Sea Interaction over the Global Oceans. *J. Climate*, 15, 2205–2231.

Allan R. P., A. Slingo, and M. A., Ringer, Influence of Dynamics on the Changes in Tropical Cloud Radiative Forcing during the 1998 El Niño, *J. Climate*, 15, 1979-1986 (2002).

Ashok, K., Behera, S. K., Rao, S. A., Weng, H. & Yamagata, T., El Niño Modoki and its possible teleconnection. *J. Geophys. Res*. 112, C11007, doi:10.1029/2006JC003798 (2007).

Bony, S., J.-L. Dufresne, H. LeTreut, J.-J. Morcrette, and C. Senior, On dynamic and thermodynamic components of cloud changes, *Clim. Dyn*., **22**, 71–86 (2004).

Bony S., J.-L. Dufresne, Marine boundary layer clouds at the heart of tropical cloud feedback uncertainties in climate models, *Geophys. Res. Lett*., **32**, L20806, doi:10.1029/2005GL023851 (2005).

Cess, R. D., M. Zhang, B. A. Wielicki, D. F. Young, X. Zhou, and Y. Nikitenko, 2001: The influence of the 1998 El Niño upon cloud radiative forcing over the Pacific warm pool. *J. Climate*, 14, 2129–2137.

Clement, A. C., R. Burgman, J. R. Norris, 2009: Observational and Model Evidence for Positive Low-Level Cloud Feedback, *Science*, 325, DOI: 10.1126/science.1171255.

Dessler, A., A determination of the cloud feedback from climate variations over the past decade, *Science*, **330**, 1523-1527 (2010).

Gu, G., R. F. Adler, G. J. Huffman, S. Curtis, Tropical rainfall variability on interannual-to-interdecadal and longer time scales derived from the GPCP monthly product, *J. Climate*, 4033-4046, DOI: 10.1175/JCLI4227.1, 2007.

Hartmann, D. L. and M. L. Michelsen, 1993: Large-scale effects on the regulation of tropical sea surface temperature. *J. Climate*, 6, 2049–2062.

Held I. M., and B. J. Soden, Robust responses of the hydrological cycle to global warming, *J. Clim*, **19**, 5686-5699 (2006).

Hoerling, Martin P., Arun Kumar, Min Zhong, 1997: El Niño, La Niña, and the Nonlinearity of Their Teleconnections. *J. Climate*, 10, 1769–1786.

Jiang, J.H., H. Su, C. Zhai, et al., Evaluation of Cloud and Water Vapor Simulations in IPCC AR5 Climate Models Using NASA 'A-Train' Satellite Observations, *J. Geophys. Res*., in review (2012).

Kao, H.-Y. & Yu, J.-Y., Contrasting Eastern-Pacific and Central-Pacific types of ENSO. *J. Clim*. 22, 615–632 (2009).

Kim, H., P. J. Webster, J. A. Curry, Impact of Shifting Patterns of Pacific Ocean Warming on North Atlantic Tropical Cyclones, *Science*, 325, 77, DOI: 10.1126/science.1174062 (2009).

Kug, J.-S., Jin, F.-F. & An, S.-I., Two types of El Niño events: cold tongue El Niño and warm pool El Niño. *J. Clim*. 22, 1499–1515 (2009).

Latif, M., Kleeman, R. & Eckert, C. Greenhouse warming, decadal variability, or El Niño? An attempt to understand the anomalous 1990s. *J. Clim*. 10, 2221–2239, (1997).

Lee, T., M. J. McPhaden, Increasing intensity of El Niño in the central‐equatorial Pacific, Geophys. Res. Lett., 37, L14603, doi:10.1029/2010GL044007 (2010).

Lindzen, R. S., and S. Nigam (1987). On the role of sea surface temperature gradients in forcing low level winds and convergence in the tropics. *J. Atmos. Sci*., 44, 2418-2436.

Loeb, Norman G., et al., 2007: Angular Distribution Models for Top-of-Atmosphere Radiative Flux Estimation from the Clouds and the Earth’s Radiant Energy System Instrument on the

454 Terra Satellite. Part II: Validation. *J. Atmos. Oceanic Technol*., **24**, 564–584. doi:
455 10.1175/JTECH1983.1.
456 Merryfield, W. J., 2006: Changes to ENSO under CO_2 Doubling in a Multimodel Ensemble. *J.*
457 *Climate*, 19, 4009–4027 (2006).
458 Mitas, C. M., and A. Clement, Has the Hadley cell been strengthening in recent decades?,
459 *Geophys. Res. Lett*., **32**, L03809 doi:10.1029/2004GL021765 (2005).
460 Oort A H, Yienger J J: Observed interannual variability in the Hadley Circulation and its
461 connection to ENSO. *J. Climate*, **9**: 2751–2767 (1996).
462 Ramanathan, V., and W. Collins, 1991: Thermodynamic regulation of ocean warming by cirrus
463 clouds deduced from observations of the 1987 El Niño. *Nature,* 351, 27–32.
464 Su, H., J. D. Neelin, and C. Chou, 2001: Tropical teleconnection and local response to SST
465 anomalies during the 1997-1998 El Niño. *J. Geophys. Res*., 106, No. D17, 20,025-20,043.
466 Su, H., and J. D. Neelin, 2003: The scatter in tropical average precipitation anomalies. *J.*
467 *Climate*, 16, 3966–3977.
468 Tanaka, H.L., et al., Trend and interannual variability of Walker, monsoon and Hadley
469 circulations defined by velocity potential in the upper troposphere. *Tellus*, **56**, 250–269 (2004).
470 Quan, X. W., et al., Change of the tropical Hadley cell since 1950. The Hadley Circulation: Past,
471 Present, and Future, H. F. Diaz and R. S. Bradley, Eds., Cambridge Univ. Press, New York,
472 85-120 (2004).
473 Weng, H., K. Ashok, S. K. Behera, S. A. Rao, T. Yamagata, Impacts of recent El Niño Modoki
474 on dry/wet conditions in the Pacific rim during boreal summer, *Clim. Dyn*., 29, 113-129
475 (2007).
476 Weng, H., Behera, S. K. & Yamagata, T. Anomalous winter climate conditions in the Pacific
477 Rim during recent El Niño Modoki and El Niño events. *Clim. Dyn*. 32, 663–674 (2009).

Williams K. D., et al., Evaluating the cloud response to climate change and current climate variability. *Clim. Dyn.* **20**,705–721 (2003).

Yeh, S. - W., J. - S. Kug, B. Dewitte, M. - H. Kwon, B. Kirtman, and F. - F. Jin, El Niño in a changing climate, Nature, 461, 511–514, doi:10.1038/nature08316 (2009).

Yuan, Jian, Dennis L. Hartmann, Robert Wood, 2008: Dynamic Effects on the Tropical Cloud Radiative Forcing and Radiation Budget. *J. Climate*, 21, 2337–2351.

Zelinka, M. D., and D. L. Hartmann, 2011, The observed sensitivity of high clouds to mean surface temperature anomalies in the tropics, *J. Geophys. Res*., 116, D23103, doi:10.1029/2011JD016459 (2011).

Zhang, M. H., R. D. Cess, S. C. Xie, Relationship between Cloud Radiative Forcing and Sea Surface Temperatures over the Entire Tropical Oceans. *J. Clim.*, 9, 1374–1384 (1996).

Table 1. The longwave (LW), shortwave (SW) and net (NET) cloud radiative forcing (CRF, in W m^{-2}) anomalies from CERES on Terra and CERES on Aqua, averaged for the tropical-mean (30°S-30°N), tropical ascending ($\omega_{500} < 0$) and descending ($\omega_{500} > 0$) regimes separately during the 2006-07 and 2009-10 DJF. Positive (negative) sign indicates warming (cooling) to the Earth-atmosphere system. The anomalies are relative to the four DJFs from 2006-2010.

	2006-07 DJF			**2009-10 DJF**		
	tropics	**$\omega_{500} < 0$**	**$\omega_{500} > 0$**	**tropics**	**$\omega_{500} < 0$**	**$\omega_{500} > 0$**
CERES-Terra LW	0.34	0.22	0.12	–0.05	–0.12	0.08
CERES-Terra SW	–0.14	–0.52	0.39	–0.57	–0.07	–0.51
CERES-Terra NET	0.20	–0.30	0.51	–0.62	–0.19	–0.43
CERES-Aqua LW	0.27	0.13	0.14	–0.22	–0.27	0.05
CERES-Aqua SW	0.19	–0.54	0.74	–0.48	0.14	–0.63
CERES-Aqua NET	0.46	–0.41	0.88	–0.70	–0.13	–0.58

Figure Captions:

Figure 1. Horizontal maps of SST anomalies during December-January-February (DJF) 2006-07 and 2009-10. The anomalies are relative to the four DJF mean from 2006 to 2010.

Figure 2. Tropical-mean anomalies of cloud water content (left) and cloud fraction (right) profiles from CloudSat/CALIPSO for the four DJFs from 2006 to 2009. The anomalies are relative to the four DJF means. Only oceanic regions between the 30ºS-30ºN are averaged. The tropical-mean sea surface temperature anomalies for the four winters are shown in the inset of Figure 2a.

Figure 3. Horizontal maps of cloud anomalies at four vertical levels (cloud water content in shadings, cloud fraction in contours) for DJF 2006-07 (left) and 2009-10 (right).

Figure 4. Horizontal maps of cloud fraction anomalies from ISCCP for December 2006 (left) and 2009 (right). The anomalies in the first and third rows are relative to the mean from 1983 to 2009, while the second and fourth rows are relative to the mean from 2006-2009. Middle and low cloud fractions are summed together due to the uncertainty in low cloud top height identification in the ISCCP data.

Figure 5. Longitude-height section of tropical-mean (10ºS-10ºN) cloud anomalies (cloud water content in shadings, cloud fraction in contours) during DJF 2006-07 and 2009-10, superimposed with ECMWF interim analysis winds. The vertical pressure velocity (in hPa/day) is enlarged 5000 times relative to the horizontal wind (in m/s).

Figure 6. Latitude-height section of zonal mean (0ºS-360ºN) cloud anomalies (cloud water content in shadings, cloud fraction in contours) during DJF 2006-07 and 2009-10, superimposed with ECMWF interim analysis winds. The vertical pressure velocity (in hPa/day) is enlarged 5000 times relative to the horizontal wind (in m/s).

Figure 7. Tropical clouds and cloud anomalies during the two El Niños sorted as a function of vertical pressure velocity at 500 hPa (ω_{500}). Color shadings for cloud water content and contours for cloud fraction. The solid curves in (a)-(b) are four DJF mean probability density function (pdf) of ω_{500}. Top panels for clouds and bottom panels for cloud anomalies relative to the four DJF mean.

Figure 8. Three components of the cloud changes as a function of ω_{500} for the two El Niños. (a) and (d): dynamic component; (b) and (e): thermodynamic component; (c) and (f): co-variations.

Figure 9. Changes in tropical circulation and SST anomaly pattern during the four DJFs. (a) The changes in the pdf of ω_{500} for two El Niños. (b) The changes in the spatial variances of $\omega_{500,}$ including zonally symmetric and asymmetric components, for the four DJFs.

Figure 10. Changes in the histograms of SST departure from the tropical mean SST for the two El Niños, (top) Observed, (bottom) Manipulated so that the tropical-mean SST anomalies were the same in DJF 2006-07 and 2009-10. See text for details.

Figure 11. Horizontal maps of top-of-atmosphere (TOA) cloud forcing anomalies from Terra CERES for DJF 2006-07 (left) and 2009-10 (right). (top row) longwave cloud forcing (LWCF), (second row) shortwave cloud forcing (SWCF), (third row) net cloud forcing, and (bottom row) the ratio N = –SWCF/LWCF. The anomalies are relative to the four DJFs from 2006 to 2010. The white areas indicate values of cloud forcing anomalies within ±0.02 W/m2, and N anomalies within ±0.02.

Figure 12. Changes of top-of-the-atmosphere (TOA) cloud forcing as a function of ω_{500} for the two El Niños. The tropical-mean TOA net (NET), longwave (LW) and shortwave (SW) CRFs are shown on the right-most panels. The top (bottom) panels use the radiative flux data from CERES on Terra (Aqua).

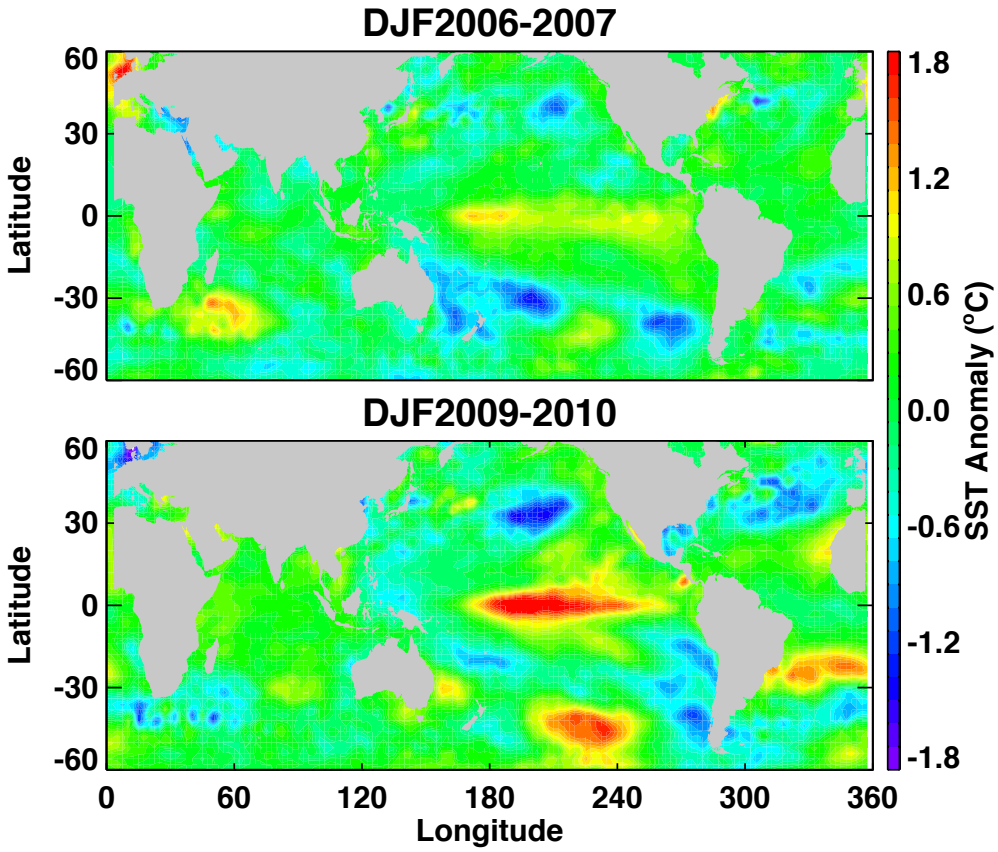

Figure 1: Horizontal maps of SST anomalies during December-January-February (DJF) 2006-07 and 2009-10. The anomalies are relative to the four DJF mean from 2006 to 2010.

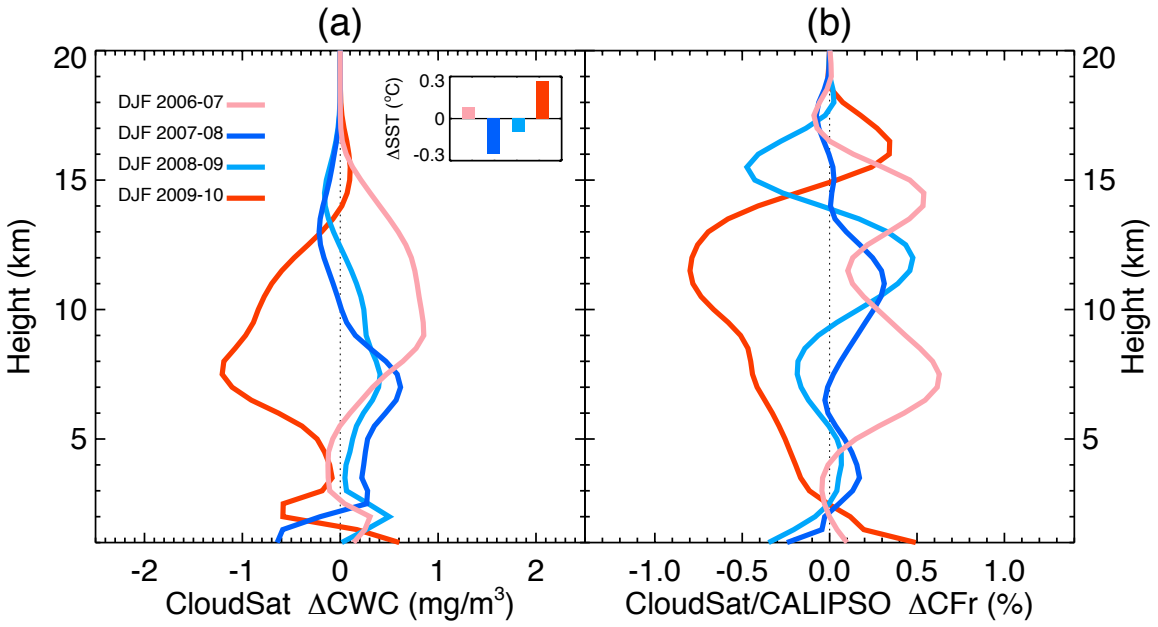

Figure 2: Tropical-mean anomalies of cloud water content (left) and cloud fraction (right) profiles from CloudSat/CALIPSO for the four DJFs from 2006 to 2009. The anomalies are relative to the four DJF means. Only oceanic regions between the 30ºS-30ºN are averaged. The tropical-mean sea surface temperature anomalies for the four winters are shown in the inset of Figure 2a.

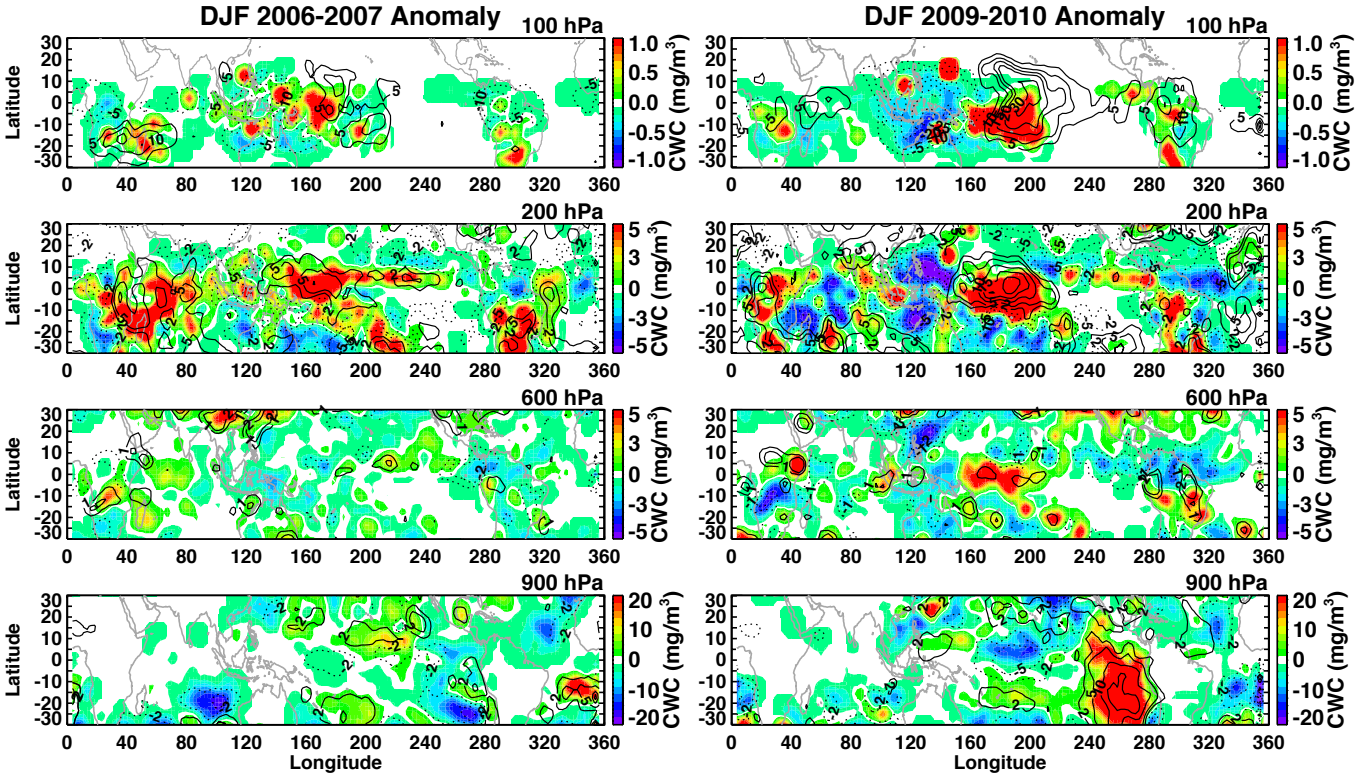

Figure 3: Horizontal maps of cloud anomalies at four vertical levels (cloud water content in shadings, cloud fraction in contours) for DJF 2006-07 (left) and 2009-10 (right).

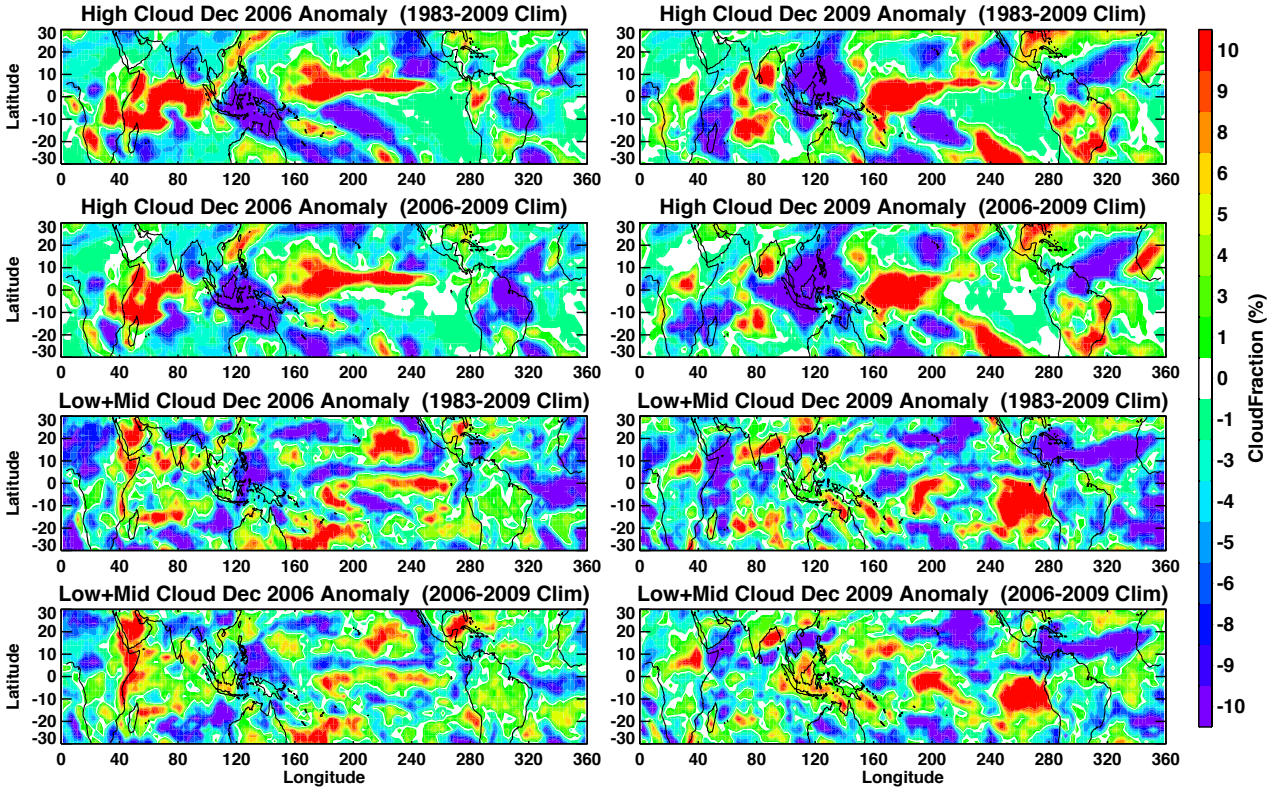

Figure 4: Horizontal maps of cloud fraction anomalies from ISCCP for December 2006 (left) and 2009 (right). The anomalies in the first and third rows are relative to the mean from 1983 to 2009, while the second and fourth rows are relative to the mean from 2006-2009. Middle and low cloud fractions are summed together due to the uncertainty in low cloud top height identification in the ISCCP data.

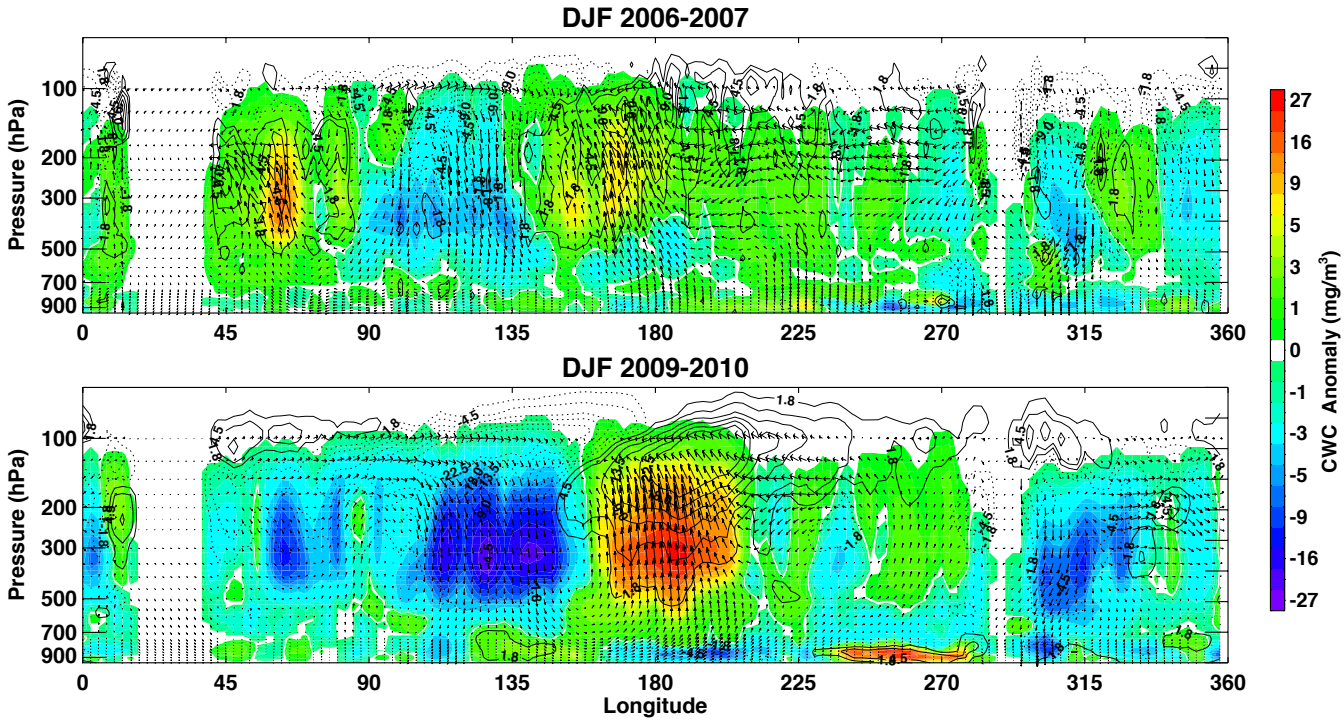

Figure 5: Longitude-height section of tropical-mean (10ºS-10ºN) cloud anomalies (cloud water content in shadings, cloud fraction in contours) during DJF 2006-07 and 2009-10, superimposed with ECMWF interim analysis winds. The vertical pressure velocity (in hPa/day) is enlarged 5000 times relative to the horizontal wind (in m/s).

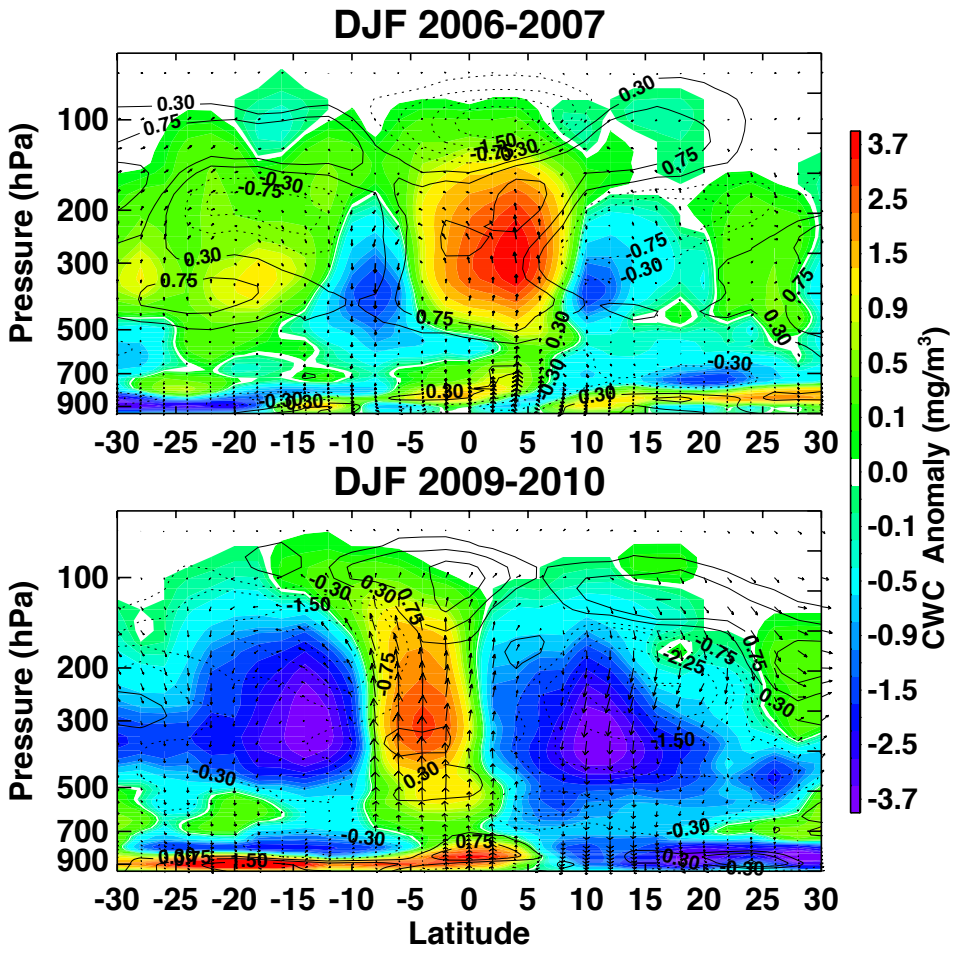

Figure 6: Latitude-height section of zonal mean (0ºS-360ºN) cloud anomalies (cloud water content in shadings, cloud fraction in contours) during DJF 2006-07 and 2009-10, superimposed with ECMWF interim analysis winds. The vertical pressure velocity (in hPa/day) is enlarged 5000 times relative to the horizontal wind (in m/s).

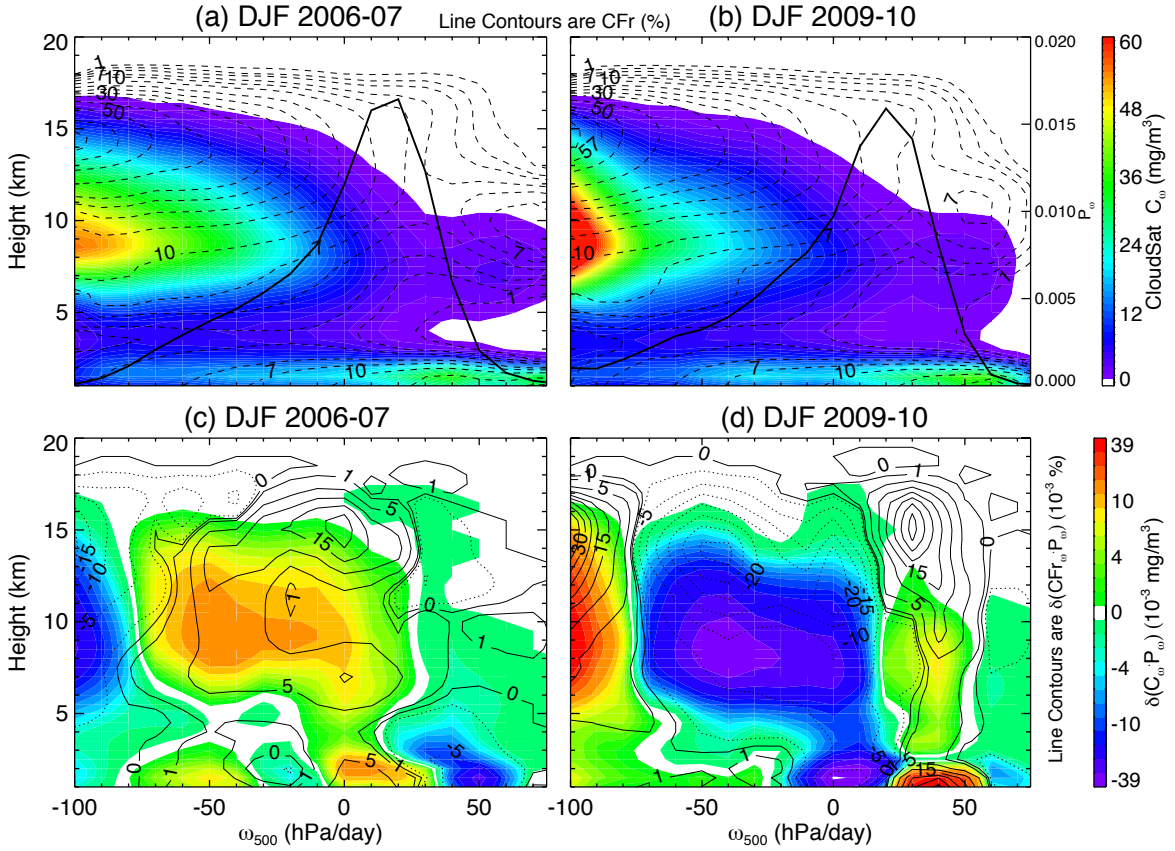

Figure 7: Tropical clouds and cloud anomalies during the two El Niños sorted as a function of vertical pressure velocity at 500 hPa (ω500). Color shadings for cloud water content and contours for cloud fraction. The solid curves in (a)-(b) are four DJF mean probability density function (pdf) of ω500. Top panels for clouds and bottom panels for cloud anomalies relative to the four DJF mean.

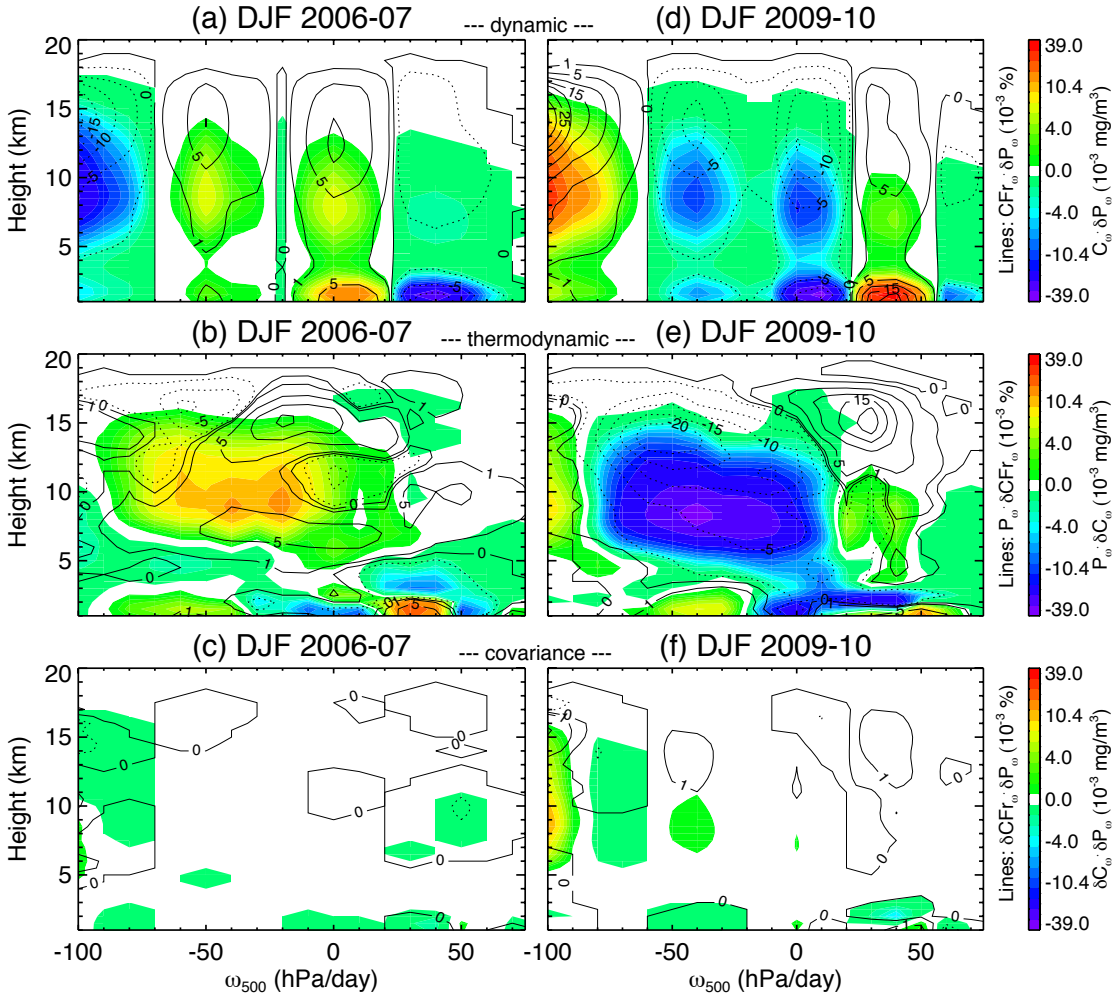

Figure 8: Three components of the cloud changes as a function of ω500 for the two El Niños. (a) and (d): dynamic component; (b) and (e): thermodynamic component; (c) and (f): co-variations.

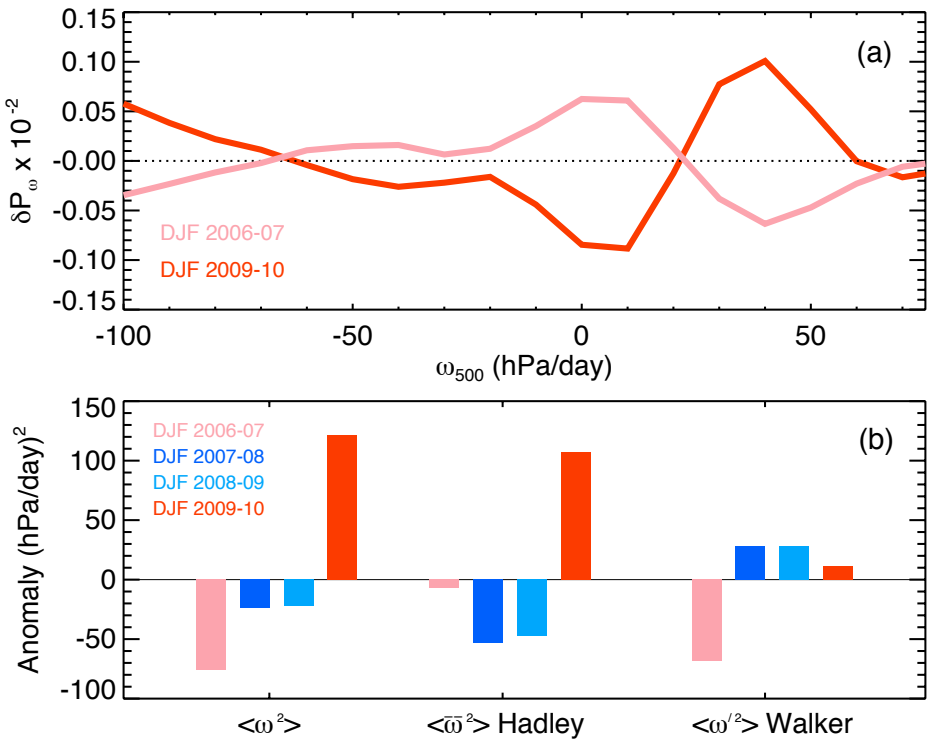

Figure 9: Changes in tropical circulation and SST anomaly pattern during the four DJFs. (a) The changes in the pdf of ω500 for two El Niños. (b) The changes in the spatial variances of ω500, including zonally symmetric and asymmetric components, for the four DJFs.

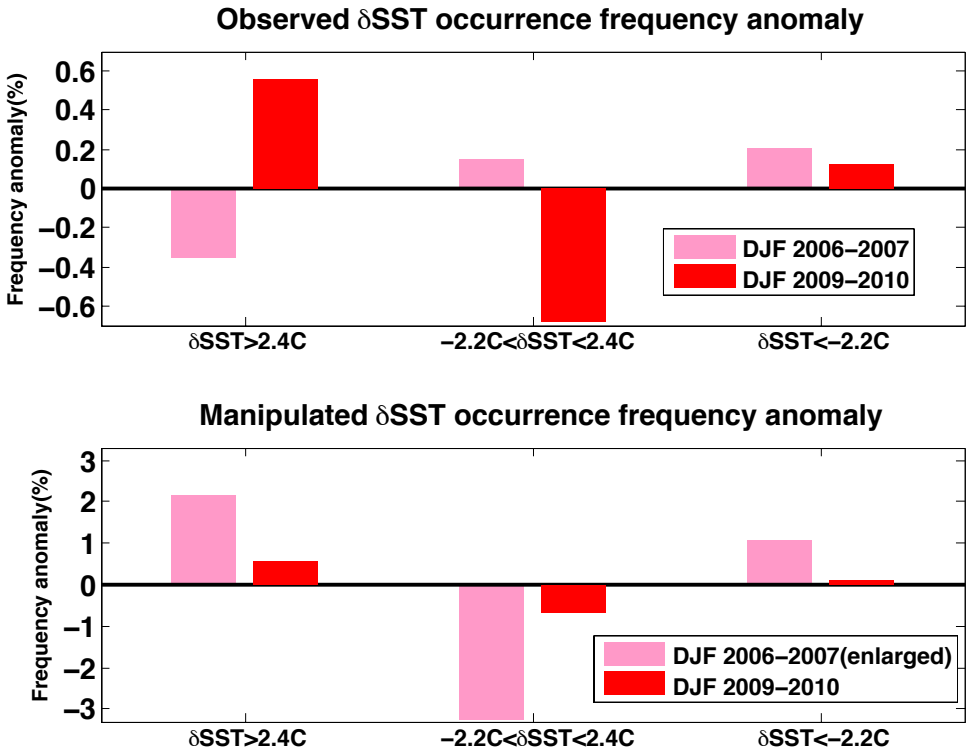

Figure 10: Changes in the histograms of SST departure from the tropical mean SST for the two El Niños, (top) Observed, (bottom) Manipulated so that the tropical-mean SST anomalies were the same in DJF 2006-07 and 2009-10. See text for details.

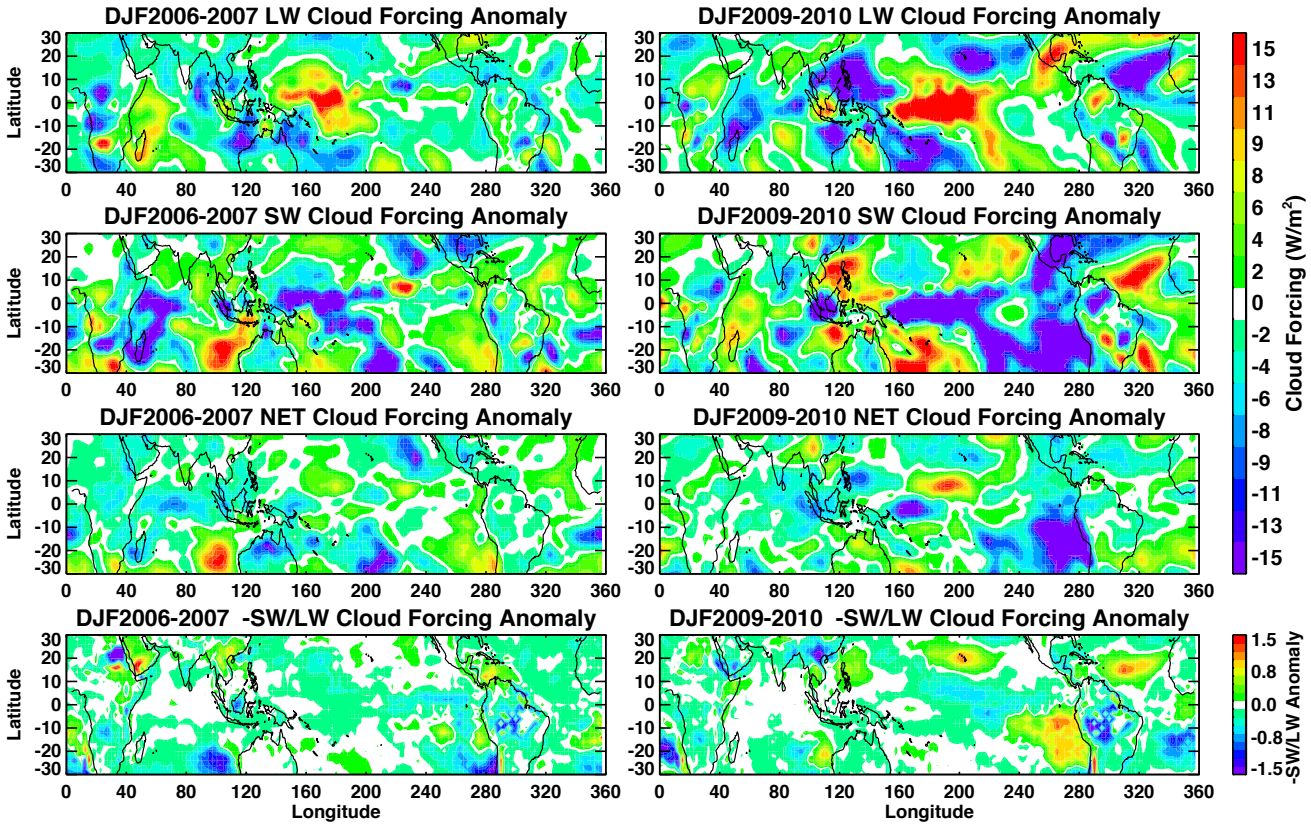

Figure 11: Horizontal maps of top-of-atmosphere (TOA) cloud forcing anomalies from Terra CERES for DJF 2006-07 (left) and 2009-10 (right). (top row) longwave cloud forcing (LWCF), (second row) shortwave cloud forcing (SWCF), (third row) net cloud forcing, and (bottom row) the ratio N = –SWCF/LWCF. The anomalies are relative to the four DJFs from 2006 to 2010. The white areas indicate values of cloud forcing anomalies within ±0.02 W/m2, and N anomalies within ±0.02.

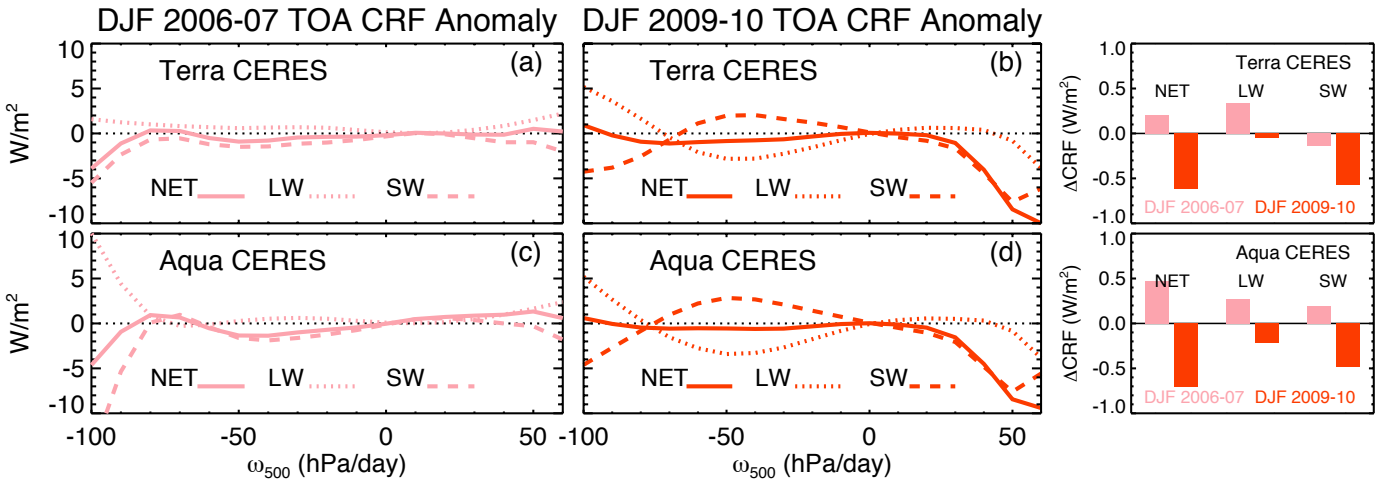

Figure 12: Changes of top-of-the-atmosphere (TOA) cloud forcing as a function of ω500 for the two El Niños. The tropical-mean TOA net (NET), longwave (LW) and shortwave (SW) CRFs are shown on the right-most panels. The top (bottom) panels use the radiative flux data from CERES on Terra (Aqua).